The geometry of decision-making in individuals and collectives

Vivek H. Sridhar[a,b,c,1], Liang Li[a,b,c,1], Dan Gorbonos[a,b,c], Máté Nagy[a,b,c,d,e,f], Bianca R. Schell[g], Timothy Sorochkin[h,i], Nir S. Gov[i], and Iain D. Couzin[a,b,c,1]

[a]Department of Collective Behaviour, Max Planck Institute of Animal Behavior, 78464 Konstanz, Germany; [b]Centre for the Advanced Study of Collective Behaviour, University of Konstanz, 78464 Konstanz, Germany; [c]Department of Biology, University of Konstanz, 78464 Konstanz, Germany; [d]MTA-ELTE "Lendület" Collective Behaviour Research Group, Eötvös Loránd Research Network, 1117 Budapest, Hungary; [e]Department of Biological Physics, Eötvös Loránd University, 1117 Budapest, Hungary; [f]MTA-ELTE Statistical and Biological Physics Research Group, Eötvös Loránd Research Network, 1117 Budapest, Hungary; [g]Department of Chemistry, University of Konstanz, 78464 Konstanz, Germany; [h]Department of Physics and Astronomy, University of Waterloo, Waterloo, ON N2L 3G1, Canada; and [i]Department of Chemical and Biological Physics, Weizmann Institute of Science, Rehovot 76100, Israel

Choosing among spatially distributed options is a central challenge for animals, from deciding among alternative potential food sources or refuges to choosing with whom to associate. Using an integrated theoretical and experimental approach (employing immersive virtual reality), we consider the interplay between movement and vectorial integration during decision-making regarding two, or more, options in space. In computational models of this process, we reveal the occurrence of spontaneous and abrupt "critical" transitions (associated with specific geometrical relationships) whereby organisms spontaneously switch from averaging vectorial information among, to suddenly excluding one among, the remaining options. This bifurcation process repeats until only one option—the one ultimately selected—remains. Thus, we predict that the brain repeatedly breaks multichoice decisions into a series of binary decisions in space–time. Experiments with fruit flies, desert locusts, and larval zebrafish reveal that they exhibit these same bifurcations, demonstrating that across taxa and ecological contexts, there exist fundamental geometric principles that are essential to explain how, and why, animals move the way they do.

ring attractor | movement ecology | navigation | collective behavior | embodied choice

Animals constantly face the need to make decisions, and many such decisions require choosing among multiple spatially distributed options. Despite this, most studies have focused on the outcome of decisions (1–3) (i.e., which option among alternatives is chosen), as well as the time taken to make decisions (4–6), but seldom on the movement of animals throughout the decision-making process. Motion is, however, crucial in terms of how space is represented by organisms during spatial decision-making; the brains of a wide range of species, from insects (7, 8) to vertebrates (9, 10), have been shown to represent egocentric spatial relationships, such as the position of desired targets, via explicit vectorial representation (11, 12). Such neuronal representations must, and do, change as animals move through space. Thus, while the movement of an animal may, initially, appear to simply be a readout of the decision made by the brain—and consequently, not particularly informative—this view overlooks important dynamical properties introduced into the decision-making process that result from the inevitable time-varying geometrical relationships between an organism and spatially distributed options (i.e., potential "targets" in space).

Due to a dearth of existing studies and with the objective to develop the necessary foundational understanding of the "geometry" of decision-making, we focus here—first theoretically and then experimentally—on the consequences of the recursive interplay between movement and (collective) vectorial integration in the brain during relatively simple spatial decisions. We employ immersive virtual reality to investigate decision-making regarding multiple (two or more) options in both invertebrate (the fruit fly *Drosophila melanogaster* and the desert locust *Schistocerca gregaria*) and vertebrate (larval zebrafish *Danio rerio*) models. Doing so allows us to reveal the emergence of geometric principles that transcend the study organism and the decision-making context and thus, are expected to be broadly relevant across taxa. In support of this finding, we also explore how these principles extend to collective decision-making in mobile animal groups, allowing us to gain insights across three scales of biological organization from neural dynamics to both individual and collective decision-making.

Modeling Decision-Making on the Move

Congruent with neurobiological studies of the invertebrate and vertebrate brain, we consider organisms to have an egocentric vectorial representation of spatial options (11–13). We then consider the collective dynamics of vector integration in the brain assuming there exists reinforcement (excitation/positive feedback) among neural ensembles that have similar directional representations (goal vectors) and global inhibition and/or negative feedback (both produce broadly similar results) (*SI Appendix*, Fig. S1) among neural ensembles that differ in

---

Significance

Almost all animals must make decisions on the move. Here, employing an approach that integrates theory and high-throughput experiments (using state-of-the-art virtual reality), we reveal that there exist fundamental geometrical principles that result from the inherent interplay between movement and organisms' internal representation of space. Specifically, we find that animals spontaneously reduce the world into a series of sequential binary decisions, a response that facilitates effective decision-making and is robust both to the number of options available and to context, such as whether options are static (e.g., refuges) or mobile (e.g., other animals). We present evidence that these same principles, hitherto overlooked, apply across scales of biological organization, from individual to collective decision-making.

vectorial representation. This captures, in a simple mathematical formulation, the essence of both explicit ring attractor networks [as found in insects (7)] and computation among competing neural groups [as in the mammalian brain (14)]. The animal's relative preference for a target is given by the activity of neurons that encode direction to that target relative to the activity of neurons that encode direction to other targets, and the angular sensitivity of the neural representations (angular difference at which excitation no longer occurs) is specified by a neural tuning parameter, ν. The network then computes a unique "consensus" vector ("activity bump") that, along with some angular noise, represents the animal's desired direction of movement (*SI Appendix*, Fig. S2). This is then translated into motor output [*SI Appendix* has model details (15)]. Stochasticity in neural dynamics is implemented here as the neural noise parameter, T.

While capturing known, generic features of neural integration, our model is deliberately minimal. This serves multiple purposes. First, following principles of maximum parsimony, we seek to find a simple model that can both predict and explain the observed phenomena. Second, we aim to reveal general principles and thus, consider features that are known to be valid across organisms irrespective of inevitable difference in structural organization of the brain. Third, it provides a convenient means to implement neural noise and can be mapped to the class of neural ring attractor models widely used in neuroscience (16–19) (*SI Appendix* has details). In addition, our results are shown to be extremely robust to model assumptions, suggesting that it provides an appropriate low-level description of essential system properties.

Deciding between Two Options

Beginning with the simplest case, we consider the feedback between motion and internal vectorial computation when an animal is presented with two equally attractive, but spatially discrete, options. In this case, the activity of neurons encoding option 1, N_1, will be equal to those encoding option 2, N_2 (Fig. 1*A*). Our model predicts that an animal moving from a relatively distant location toward the two targets will spontaneously compute the average directional preference, resulting in corresponding motion in a direction oriented between the two targets. As it approaches the targets, however, upon reaching a certain angular difference between the options, the internal network undergoes a sudden transition in which it spontaneously selects one or the other target (Fig. 1*C*). This results in an abrupt change in trajectory: the animal being redirected toward the respective "selected" target (Fig. 1*C*; *SI Appendix*, Fig. S3*A* shows the same phenomenon occurring for a wide range of starting positions).

Our model, therefore, predicts that despite the fact that the egocentric geometrical relationship between the animal and the targets changes continuously, upon approaching the targets there exists a location whereby a further very small increase in angular difference between the targets will result in a sudden change in system (neural) dynamics and consequently, in motion and thus, decision-making. Such spatiotemporal dynamics do not occur if individuals were to simply integrate noisy vectorial information or choose their travel direction from a summed distribution of the location of targets in their sensory field (20), points we will return to later.

In numerical analysis of our model, we find that irrespective of starting position, as the animal reaches the respective angle
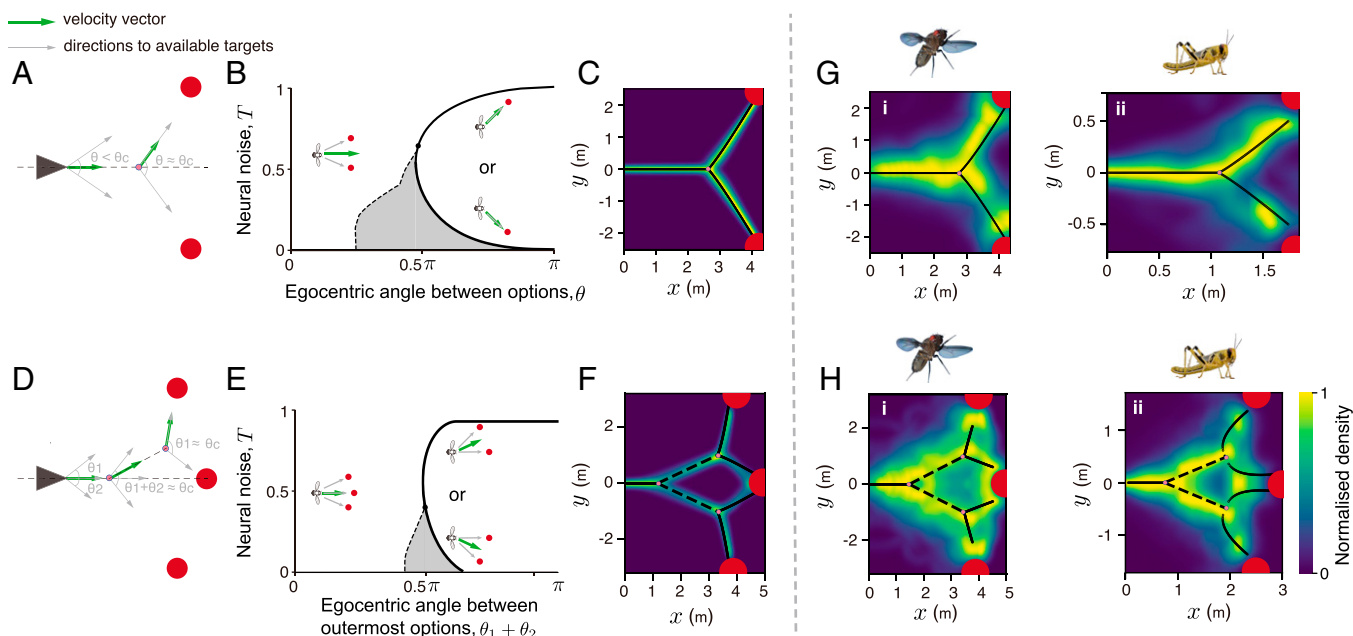
Fig. 1. Geometrical principles of two-choice and three-choice decision-making. (*A*) Schematic of the binary decision-making experiments. This simplified representation shows that a sharp transition in the animal's direction of travel is expected near a critical angle, θ_c. (*B*) A phase diagram describing the "critical" transition exhibited while moving from compromise to decision between two options in space. The shaded area (also in *E*) represents the region in parameter space where both the compromise and the decision solutions exist. (*C*) Density plot showing trajectories predicted by the neural model in a two-choice context. The axes represent *x* and *y* coordinates in Euclidean space. The black line (also in *G*) presents a piecewise phase transition function fit to the bifurcation. (*D*) Schematic of three-choice decision-making experiments, where the central target is on the angle bisector of the angle subtended by the other two targets. (*E*) A phase diagram describing the first critical transition when the individual chooses among three options. After the individual eliminates one of the outermost targets, it can decide between the two remaining options, similar to the two-choice phase diagram described in *B*. (*F*) Theoretical predictions for decision-making in a three-choice context. The dashed line (also in *H*) is the bisector of the angle subtended by center target and the corresponding side target on the first bifurcation point. *SI Appendix*, Table S1 shows the parameters used in *C* and *F*. (*G* and *H*) Density plots from experiments conducted with flies (*i*) and locusts (*ii*) choosing among two and three options, respectively. Note that the density plots presented here are for the nondirect tracks, which constitute the majority type of trajectory adopted by both flies and locusts (*SI Appendix*, Figs. S11 and S12). However, our conclusions do not differ if we use all unfiltered data (*SI Appendix*, Figs. S11 *G* and *N* and S12 *I* and *R*).

2 of 8 | PNAS
https://doi.org/10.1073/pnas.2102157118

Sridhar et al.
The geometry of decision-making in individuals and collectives

in space, it will relatively suddenly select one of the options (*SI Appendix*, Fig. S3*A*). While the specific angular difference at which this phenomenon occurs is dependent on neural tuning, ν (*SI Appendix*, Fig. S3*C*), and the starting configuration, (*SI Appendix*, Fig. S3*B*) (due to an interplay between the two timescales involved), it is always present as long as the neural noise, T, remains below a critical firing rate, T_c (although even for $T < T_c$, these bifurcations may be difficult to see for small values of ν due to inherent noise in real biological systems) (*SI Appendix*, Fig. S4 shows simulations where vectorial representations of targets include directional error).

To gain a deeper insight into the mechanism underlying the observed spatiotemporal dynamics, we constructed a mean-field approximation of our model (*SI Appendix*) since this has the advantage of allowing us to conduct formal analyses of patterns realized in the simulated trajectories.

Geometric Principles of Decision-Making

The mean-field analysis of our model shows that below a critical level of neural noise, animals will adopt the average among options as they approach the targets until a critical phase transition upon which the system spontaneously switches to deciding among the options (Fig. 1*B* and *SI Appendix*, Fig. S5*A*). Thus, despite varying in its exact location (Fig. 1*B*), the sudden transition observed is an inevitable consequence of the system dynamics and will always occur.

Such sudden transitions correspond to "bifurcations" in the mathematical study of dynamical systems. A bifurcation is said to occur when a smooth change in an external parameter, in this case perceived angular difference between the options, causes a sudden qualitative change in the system's behavior, here corresponding to a literal bifurcation (or branching) in physical space.

When dynamical systems undergo such a phase, or quasiphase, transition, they exhibit a remarkable universal property; close to the transition, at the "critical point" or "tipping point," the system spontaneously becomes extremely sensitive to very small perturbations [e.g., to small differences in preference between options (21, 22)]. This is true of both physical [e.g., magnetic (23)] and biotic [e.g., cellular (24, 25)] systems undergoing a phase transition. Correspondingly, we find that below a critical level of neural noise, the mean-field model exhibits a sudden increase in susceptibility as the animal approaches the critical point, immediately prior to the decision being made (*SI Appendix*, Fig. S5*A*). This will not occur in previously considered models where an animal is assumed to choose its direction of travel based on the summed distribution of targets in its sensory field, also known as probability density function (PDF) sum-based models (20). Thus, as animals approach targets, we predict they will pass through a window of space (corresponding to the critical angle for the respective geometry they are experiencing) in which their brain spontaneously becomes capable of discriminating between very small differences between options (e.g., a very small difference in neuronal activity being in "favor" of one option) (*SI Appendix*, Fig. S3*D* has details). This highly valuable property (for decision-making) is not built into the model but is rather an emergent property of the inherent collective dynamics.

In many real biological systems, including the ones we consider here, the (neural) system size is typically not large enough to consider true phase transitions (which only occur for very large systems, as per the mean-field approximation) but rather, "phase transition–like" or "quasiphase transition" behavior. Even though real biological systems are not necessarily close to the infinite size limit of the mean-field approximation, we see very similar dynamics for both small and large system sizes (*SI Appendix*, Fig. S6).

Decision-Making beyond Two Options

While the majority of decision-making studies consider only two options [due to both theoretical and experimental tractability (14, 26, 27)], animals moving in real space frequently encounter a greater number than this. Here, we consider how animals will be expected to select among three, or more, options (possible targets) in space. First, we begin with three identical options ($N_1 = N_2 = N_3$) since this gives us the clearest insight into the relationship between motion and decision-making dynamics. Then, we relax these assumptions and consider differences between options (*SI Appendix*, Fig. S3*E*) as well as a greater number of options (Fig. 2). Note that we do not modify our model in any way prior to introducing these additional complexities.

Below T_c (*SI Appendix*, Fig. S7 has considerations when $T > T_c$), we once again find that the direction in which the animal moves is a function of the angular difference between the targets. When relatively far from the targets, it moves in the average of these three directions. Upon reaching a critical angular threshold between the leftmost and rightmost options (from the animal's perspective), however, the neural system spontaneously eliminates one of them, and the animal begins moving in the direction average between the two remaining options (Fig. 1 *D* and *E*). It continues in this direction until a second critical angle is reached, and now, the animal eliminates one of the two remaining options and moves toward the only remaining target (Fig. 1*F* and *SI Appendix*, Fig. S5*B*). Thus, we predict that the brain repeatedly breaks multichoice decisions into a series of binary decisions in space–time. Such bifurcation dynamics are not captured in models of decision-making that do not include the required feedbacks, such as if individuals simply sum noisy vectors (or PDFs) to targets in their sensory field (20). For the case of three targets, vectors/votes to the leftmost option would tend to cancel those that favor the rightmost option, resulting in the selection of the central option, an issue we will return to later when considering collective animal behavior. Simulating a larger
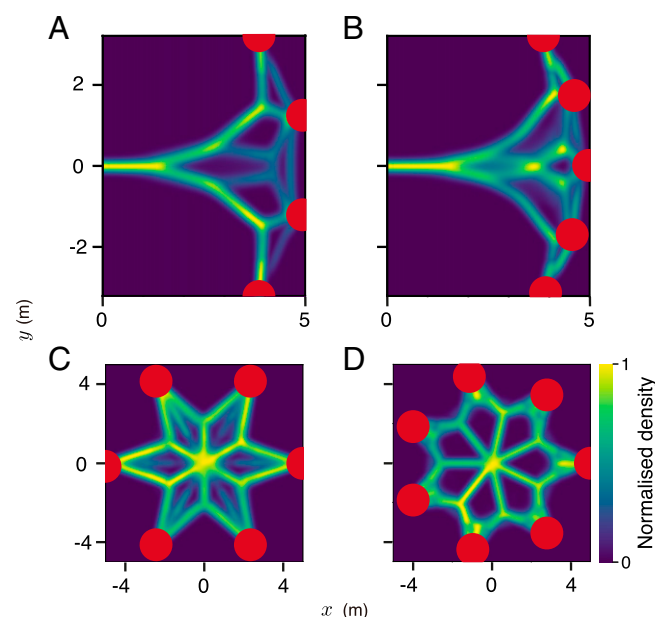
Fig. 2. Decision-making for a larger number of targets. Density plots of simulated trajectories for four- (*A*), five- (*B*), six- (*C*), and seven-choice (*D*) decision-making when targets are placed equidistant and equiangular from the agent. The axes represent *x* and *y* coordinates in Euclidean space. Geometrical configurations are also varied to place the targets on the same side of the agent (*A* and *B*) or in radial symmetry (*C* and *D*). *SI Appendix*, Table S1 shows the parameters used in *A*–*C*. In *D*, all parameters used are identical except the system size $N = 70$.

Sridhar et al.
The geometry of decision-making in individuals and collectives

PNAS | 3 of 8
https://doi.org/10.1073/pnas.2102157118

ECOLOGY

BIOPHYSICS AND COMPUTATIONAL BIOLOGY

number of options (Fig. 2) and varying environmental geometries (*SI Appendix*, Figs. S8 and S9) demonstrate the robustness of this mechanism in the face of environmental complexity and the more complex spatial dynamics that emerge as organisms undergo repeated bifurcations.

Experimental Tests of Our Predictions

Since the decision process is predicted to be sequential and dependent on the geometry with respect to the targets from an egocentric perspective, it should be possible to visualize it directly from the trajectories taken by animals when making spatial decisions. In this respect, our theoretical studies make a key testable prediction; if neural groups within the decision-making ensemble exhibit relatively local excitation and long-range/global inhibition, we should observe bifurcations in the animals' trajectories as they choose among identical options, and if animals face three (or more) such options, then the complex decision task should be broken down to a series of binary decisions.

Since the geometrical principles revealed above are expected to be both robust and generic, we use immersive virtual reality (28) (*SI Appendix*, Fig. S10) to test our predictions by investigating both two- and three-choice decision-making in three evolutionarily highly divergent brains under ecologically relevant scenarios: fruit flies (*D. melanogaster*) and desert locusts (*S. gregaria*) deciding which among multiple vertical objects to approach (e.g., to perch) and zebrafish (*D. rerio*) choosing with which conspecific(s) to school. Like many other insects (29–32), fruit flies (33) and desert locusts (34) exhibit a natural tendency to orient and move toward high-contrast vertical features (potential landing sites or indicators of vegetation) in their environment. We exploit this tendency, presenting multiple identical black pillars as targets in an otherwise white environment. We record trajectories of our focal animals (solitary flies or locusts) as they choose to move toward one of these pillars, thus obtaining a behavioral readout of the decision-making process (*SI Appendix* has experimental details; *SI Appendix*, Figs. S11 and S12 show raw trajectories of flies and locusts, respectively).

As predicted by our theory (Fig. 1 *B* and *C*), we find that, in the two-choice case, most flies and locusts that choose one of the presented targets initially move in the average of the egocentric target directions until a critical angular difference (*SI Appendix*, Fig. S13), at which point they select (randomly) one or the other option and move toward it (a randomization test where *y* coordinates between trajectories were swapped showed that the bifurcation fit to our experimental data was highly significant; $P < 0.01$ for both flies and locusts) (Fig. 1*G* and *SI Appendix*, Fig. S13). Here, we note that there may be multiple factors that affect the animals' direction of movement. For example, it could be that animals repeatedly switch between fixating on each of the two options before reaching the critical angular difference, following which they select one. However, quantification of their heading relative to the targets and to the average direction between the targets (*SI Appendix*, Fig. S13) finds no evidence for this; instead, prior to the bifurcation, both flies and locusts exhibit a heading toward the average of the egocentric target directions. In the three-choice case, the animals' movements are also consistent with our theory; as predicted (Fig. 1 *E* and *F*), they break the three-choice decision into two sequential binary decisions ($P < 10^{-4}$ for both flies and locusts) (Fig. 1*H*). For both animals, the observed angle of bifurcation ($\sim 110°$ for flies and $\sim 90°$ for locusts) is much larger than their visual spatial resolution [$\sim 8°$ and $\sim 2°$ for flies (35) and locusts (36, 37), respectively]. We note that $\sim 30\%$ of animals in our experiments (both flies and locusts) did not exhibit the sequential bifurcations (*SI Appendix*, Figs. S11 and S12) described above and instead, moved directly toward one of the presented targets (*SI Appendix*, Figs. S11 and S12). Such variability in response is expected in animals and is consistent with recent

work on the visual response of flies, which demonstrates a link between stochastic (nonheritable) variation in brain wiring within the visual system and strength of visual orientation response to a vertical stripe target (38). Furthermore, flies that experience high temperatures during development appear to exhibit a particularly strong orientation tendency, exhibiting the most direct paths to targets, while flies that experience low developmental temperatures exhibit wandering paths to targets (39). In our model, such differences can be accounted for by variation in directional tuning of the neural groups, with high directional tuning (low ν) being associated with a strong orientational response and such individuals exhibiting direct tracks to targets from the outset (*SI Appendix*, Fig. S14).

A further nonmutually exclusive possibility is that a subset of insects exhibits "handedness." For example, in ref. 40, it was shown that approximately 25% of *Drosophila* were either strongly left biased or right biased when moving on a Y maze and that these consistent differences among flies were similarly nonheritable. This experimental design did not assess whether a further subset was biased to go directly forward if offered three directional choices (such as could occur in a hypothetical Ψ maze). In such cases, it is certainly possible that these intrinsic directional biases break symmetry (*SI Appendix*, Fig. S3 *D* and *E*), resulting in directed paths to different targets.

We note that individuals predisposed to exhibit direct paths to targets would be expected to make faster, yet less accurate, decisions, a prediction we plan to test in future studies.
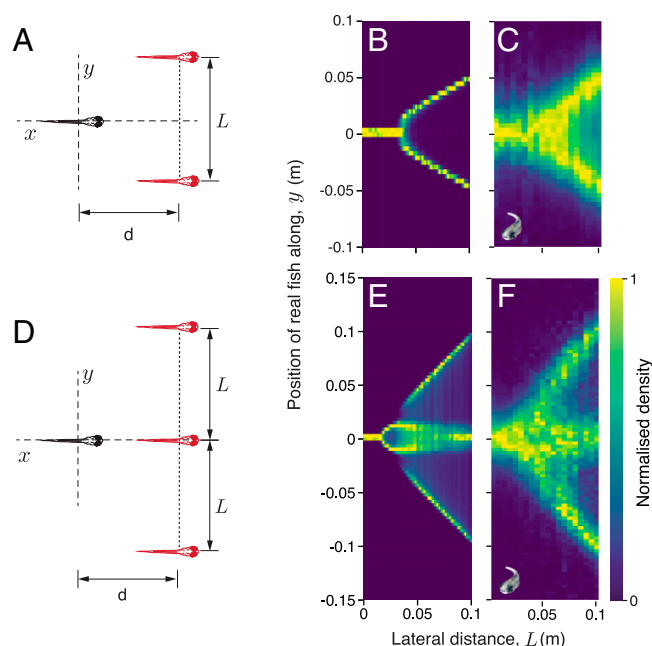
Our zebrafish experiments consider spatial decision-making in a social context. We present virtual conspecifics (*SI Appendix* has methodological details) that move back and forth in the arena parallel to each other as targets (Fig. 3*A* and *SI Appendix*, Fig. S15*A*) and behave (*SI Appendix*, Fig. S16), and are responded to (*SI Appendix*, Fig. S17), in the same way as real fish. Because they are social, the real fish respond to these virtual fish by tending to follow at a (relatively) fixed distance behind them (*SI Appendix*, Fig. S15*E*). Our data are best represented within this moving frame of reference (the virtual fish) (*SI Appendix*, Fig. S15). Theoretically, we predict that for two virtual fish, we should see a single bifurcation, where the real fish will suddenly switch from averaging the target directions to deciding among them (i.e., swimming predominantly with one of the virtual fish) as a function of increasing the lateral distance, L, between the virtual fish (Fig. 3*B* and *SI Appendix*, Fig. S18; *SI Appendix* has details of model implementation). The existence of this bifurcation is clearly seen in our experiments (Fig. 3*C*). When considering three moving virtual conspecifics, the model predicts that real fish will spontaneously break the three-choice decision to two binary decisions, and a comparison of the theoretical prediction and experimental results demonstrates this to be the case (c.f. Fig. 3 *E* and *F*).

We also test predictions under conditions where there is an asymmetric geometry whereby two fish swim closer to each other than the central one does to the third fish (Fig. 4*A*). As predicted by our theory (Fig. 4*B*), the real fish tends to swim between the two closely associated fish or close to the third more distant fish (Fig. 4*B*). Note that, also as predicted, the real fish spends a similar amount of time in each of the two locations.

Although detailed models considering the specifics of each system would be expected to provide additional quantitative fits (at the expense of losing some degree of generality and analytical tractability), our results are broadly independent of the model implementation details. Thus, we find that the key predictions of our model are validated in fruit flies, desert locusts, and larval zebrafish in distinct yet ecologically relevant contexts.

Model Features That Determine Network Behavior

There are key features that are essential to produce the bifurcation patterns observed in our data (i.e., for any decision-making

4 of 8 | PNAS
https://doi.org/10.1073/pnas.2102157118

Sridhar et al.
The geometry of decision-making in individuals and collectives

Fig. 3. Decision-making in a moving frame of reference. (*A*) Schematic of the two-choice decision-making experiments conducted with larval zebrafish. In these experiments (also in the three-choice experiments depicted in *D*), the virtual fish swim parallel to each other while maintaining a fixed lateral distance, *L*, between them. We only consider data where the real fish swims behind the virtual fish (i.e., it follows the virtual fish) (*SI Appendix*, Fig. S15 has details). (*B*) Normalized probability distribution (proportion of maximum) of simulated positions of an agent following two moving targets and corresponding experiments (*C*) conducted with larval zebrafish following two virtual conspecifics. (*D*) Schematic representation of the three-choice decision-making experiments. (*E*) Normalized probability distributions of simulated positions of an agent following three moving targets and corresponding experiments (*F*) conducted with larval zebrafish following three virtual conspecifics. *SI Appendix*, Table S1 shows the model parameters used in *B* and *E*.

system to break multichoice decisions to a series of binary decisions).

1) Feedback processes that provide the system directional persistence and drive such bifurcations are crucial to exhibit the observed spatiotemporal dynamics. In the neural system, this is present in the form of local excitation and long-range/global inhibition (7, 18, 19). However, as shown in our model of collective animal behavior below, we expect that similar dynamics will be observed if the necessary feedbacks are also incorporated into other models of decision-making, such as to PDF sum–based models, for example (20).

2) Observing similar decision dynamics requires a recursive (embodied) interplay between neural dynamics and motion in continuous space. Here, the animal's geometrical relationship with the targets changes as it moves through physical space. Since neural interactions depend on this changing relationship, space provides a continuous variable by which the individual traverses the time-varying landscape of neural firing rates.

These essential features, along with the observed animal trajectories in the two-choice context, are reminiscent of collective decision-making in animal groups [models (41–45), fish schools (46), bird flocks (47), and baboon troops (26)]. Below, we consider an established model of collective decision-making (41) to draw links between these two scales of biological organization—decision-making in the brain and decision-making in animal groups.

A Link to Collective Decision-Making

In order to draw a link between individual decision-making and collective decision-making in animal groups, we consider an animal group with an equal number of individuals exhibiting preference for each target (*SI Appendix* has methodological details). A long-standing approach in the study of animal collectives is to consider them integrating vectorial information from neighbors (48, 49), and there are a great number of publications of such "flocking," "schooling," or "herding" behaviors (48–50). Individuals within groups may also have preferences to reconcile this local vector averaging with goal-oriented behavior, such as a desired direction of travel (41, 46), and such models have made effective predictions regarding how the number of individuals with a common desired direction of travel influences the accuracy of group motion toward targets (26) and how the weighting of the internal "goal-oriented" vector representing the desired direction of travel influences the capacity and accuracy for individuals to act as leaders and to influence the direction taken by the group as a whole (51).

We demonstrate here, however, that while ubiquitous, such models of collective animal behavior fail to account for the known capability for animal groups to make decisions among spatially discrete targets (*SI Appendix*, Fig. S19 *A* and *B*). To do
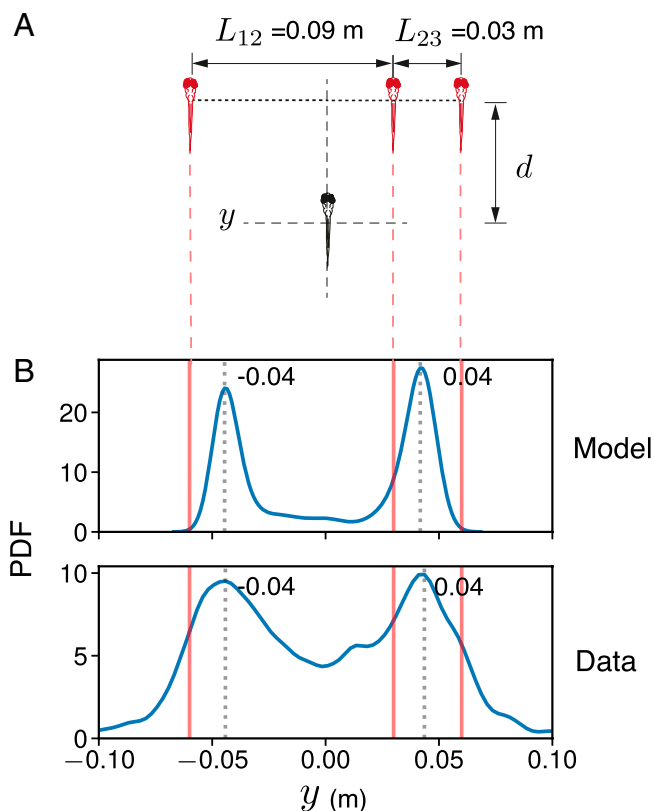
Fig. 4. Decision-making with the targets in an asymmetric geometry. (*A*) Schematic of the asymmetric choice test presented to larval zebrafish. In these experiments, the virtual fish swim parallel to each other while maintaining a fixed lateral distance, *L*, between them. To create asymmetry in the geometry, the center fish swims closer to one of the side fish than the other ($L_{12} = 0.09$ m and $L_{23} = 0.03$ m). *B*, *Upper* shows the PDF of simulated positions of an agent following three moving targets in an asymmetric geometry corresponding to the experiments. The simulated agent occupies a position of $y = \pm 0.04$ m while following the targets ($\nu = 0.7$; $\sigma_\theta = 0.3$). *B*, *Lower* shows the PDF of the position of the real fish along the axis perpendicular to its direction of motion. As predicted by our model, the real fish considers the two virtual conspecifics closer to each other as a single target and adopts one of two positions behind the virtual fish.

Sridhar et al.
The geometry of decision-making in individuals and collectives

PNAS | 5 of 8
https://doi.org/10.1073/pnas.2102157118

so, it is essential that the necessary feedbacks, as described above for collective decision-making among neurons, are incorporated. While these feedbacks are inherent to our neural model, they can also be included in other models in the form of social interactions or in the animals' response to their environment (52).

For example, one way feedback can be introduced here is via "informed" individuals (those with a desired direction of travel) associating with "uninformed" or "unbiased" individuals (individuals that exhibit social interactions but have no specific desired direction of travel) (41, 46); uninformed individuals are effectively recruitable by those with a desired direction of travel (providing local positive feedback) but are also in finite supply, creating what is effectively a competition among informed subsets that differ in their preferred direction of travel (a form of longer-range inhibition between informed subsets). However, because uninformed individuals tend to average the direction of all informed individuals that recruit them, we find that this type of feedback functions more as a social glue and is only able to explain bifurcations when the group is choosing between two options. In a decision-making context with three options, this type of feedback results in the group almost always moving toward the central target (*SI Appendix*, Fig. S19*D*).

A means of resolving this issue is for individuals to change the strength of their goal-orientedness as a function of their experienced travel direction; for example, individuals that find themselves consistently moving in a (group) direction that differs from their preferred target direction could weaken the strength of their preference over time [a form of forgetting/negative feedback, effectively resulting in long-range/global inhibition; when this preference is lost, they will tend to spontaneously reinforce the majority-selected direction (46), a form of positive feedback]. We find that this biologically plausible mechanism (41) will allow individuals within the group to recover the capability to come to consensus even in the absence of uninformed individuals (Fig. 5) and for a greater number of options than two (Fig. 5*B*).

Despite considerable differences in details between this model and that of neural dynamics described above, with the former involving individual components that change neighbor relationships over time and where inhibition emerges from a different biological process, the predictions regarding motion during decision-making are extremely similar (c.f. Figs. 1and 5show a comparison between predictions for neural groups and animal groups, respectively). Thus, we find that similar principles may underlie spatial decision-making across multiple scales of biological organization. Furthermore, by presenting social interactions in a decision-making context, our zebrafish experiments elucidate the neural basis of schooling, allowing us to glean insights across three scales of biological organization—from neural dynamics to individual decisions and from individual decisions to collective movement.

Conclusions

We demonstrate that, across taxa and contexts, explicitly considering the time-varying geometry during spatial decision-making provides insights that are essential to understand how and why animals move the way they do. The features revealed here are highly robust, and we predict that they occur in decision-making processes across various scales of biological organization, from individuals to animal collectives (Fig. 5 and *SI Appendix*, Fig. S19), suggesting they are fundamental features of spatiotemporal computation.

Materials and Methods

We construct a simple, spatially explicit model of neural decision-making to study how the brain reduces choice in the presence of numerous spatial options (adapted from ref. 15). Theoretical predictions obtained were then tested experimentally by exposing invertebrate (fruit flies and desert locusts) and vertebrate systems (zebrafish) to spatial choice tests in virtual reality. To
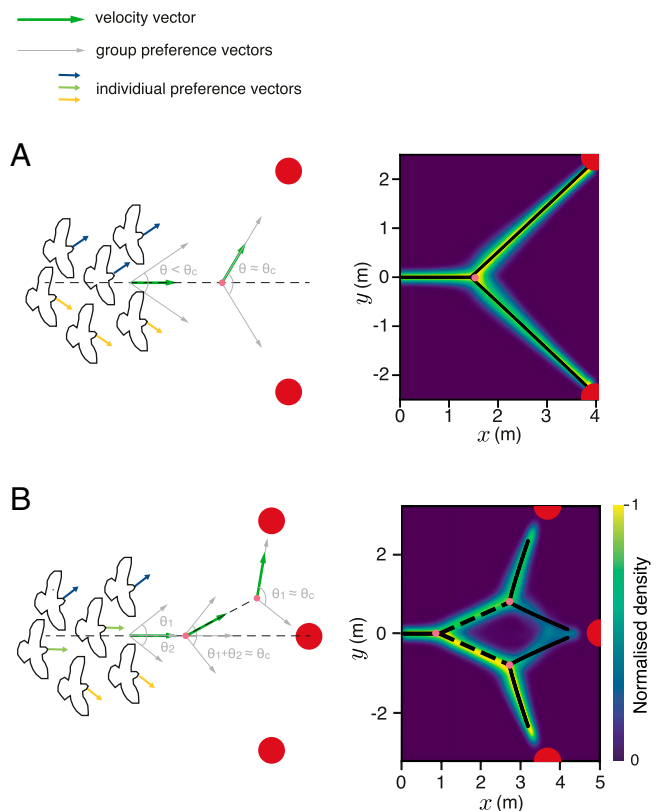
Fig. 5. Consensus decision-making in simulations of animal groups follow the same geometrical principles. Results for two- (*A*) and three-choice (*B*) decision-making in a model of animal collectives. The density plots show trajectories adopted by the centroid of the animal group for 500 replicate simulations where the groups do not split. The axes represent *x* and *y* coordinates in Euclidean space. The black lines show a piecewise phase transition function fit to the trajectories. For the three-choice case (*B*), the dashed line is the bisector of the angle subtended by the center target and the corresponding side target on the first bifurcation point. *SI Appendix*, Table S2 shows the parameters used.

identify unifying principles of spatiotemporal computation across scales of biological organization, we also reproduce the obtained decision-making patterns with an established model of collective decision-making in animal groups.

Neural Decision-Making Model. We construct a computational model of neural decision-making that takes in a representation of directions to the different targets as input and outputs a collective vectorial representation of the agent's future velocity (adapted from ref. 15). This provides us with explicit predictions for animal trajectories, allows us to determine which target is reached in each realization of the simulation, and facilitates direct comparison with experimental tests. Our model is within the class of widely employed neural ring attractor models (*SI Appendix*), which like neural field models (53, 54) and attractor network models more generally (16, 18, 55), consider the collective firing activity of the neurons, or the firing rate, as opposed to the microscopic state of each firing neuron.

In our model, the brain is composed of individual components, called "spins," that collectively, as a "spin system," represent neural activity. Spin systems, which have been long studied in physics due to their ability to give insight into a wide range of collective phenomena from magnetic to quantum systems (56), were first introduced in the study of neurobiology by Hopfield (57) in a landmark paper that provided considerable insights into principles underlying unsupervised learning and associative memory. In its simplest (and most common) formulation, as in Hopfield networks, a spin system is composed of entities, spins, that can each be in state 0 or 1 or in the terminology of physics, either "up" or "down." Spin systems have consistently provided deep insights into complex collective phenomena from spin and molecular systems to neural systems undergoing phase transitions (58, 59) (*SI Appendix* has details and discussion).

Here, the animal's brain is characterized by a system of N spins. Each spin i encodes the direction to one of the presented goals $\hat{p}_i$ and exists in one of two states: $\sigma_i = 0$ or $\sigma_i = 1$. We do not imply that a spin is equivalent to a neuron but rather, as we show via a mathematical derivation, that the collective properties of interacting spins in our model are equivalent to the firing rate in the neural ring attractor model (*SI Appendix* has details). Consequently, we refer to the individual components with which we model our system as spins and "neural activity" as a term to represent this "firing rate" equivalent. The energy of the system (for any given configuration) is given by its Hamiltonian, H:

$$H = -\frac{k}{N} \sum_{i \neq j} J_{ij} \sigma_i \sigma_j,$$ [1]

where k is the number of options available to the individual and J_{ij} is the interaction strength between spins i and j. Here, J_{ij} is given by

$$J_{ij} = \cos\left(\pi \left(\frac{|\theta_{ij}|}{\pi}\right)^{\nu}\right),$$ [2]

where θ_{ij} is the angle between preferred directions of spins i and j and ν represents the neural tuning parameter. For $\nu = 1$, the interactions become "cosine-shaped" $J_{ij} = \cos(\theta_{ij})$, and the network has a Euclidean representation of space (*SI Appendix*, Fig. S1). For $\nu < 1$, the network has more local excitation and encodes space in a non-Euclidean manner (*SI Appendix*, Fig. S1). System dynamics are implemented by energy minimization using the Metropolis–Hastings algorithm (similar to other Ising spin models), and the agent then moves with a velocity $\vec{V}$ determined by the normalized sum of goal vectors $\hat{p}_i$ of all active spins:

$$\vec{V} = \frac{v_0}{N} \sum_{i=1}^{N} \hat{p}_i \sigma_i,$$ [3]

where v_0 is the proportionality constant. The goal vector $\hat{p}_i$ of spin i now points from the agent's updated location to its preferred goal with directional noise chosen from a circularly wrapped Gaussian distribution centered at zero with an SD σ_e. As in the mean-field approximation of the model, the timescale of movement (defined by the typical time to reach the target) in the numerical simulations was set to be much greater than the timescale of neural activity (the typical time between two consecutive changes in the neural states σ_i).

Collective Decision-Making Model. We reproduce results from our neural decision-making model in a model that describes spatial decision-making at a different scale of biological organization (refer to ref. 41 for methodological details). To highlight the features that are key to producing the observed bifurcation patterns, we run simulations with and without feedback on the strength of goal-orientedness of individuals.

Fly Virtual Reality Experiments. All experiments were conducted on 3- to 5-d-old female wild-type canton special (CS) strain *D. melanogaster* raised at 26 °C on a 12-h light, 12-h dark cycle. Experiments were conducted in a fly virtual reality setup procured from loopbio GmbH (refer to ref. 28 for details). Sixty tethered *Drosophila* were exposed to either a two-choice or a three-choice decision task (30 and 30 individuals, respectively) in the virtual reality environment. Each experimental trial lasted 15 min where flies were exposed to five sets of stimuli—three experimental sets and two control sets. The experimental stimuli sets consisted of two or three black cylinders (depending on the experimental condition) that were presented to the animal in an otherwise white environment. A control stimulus with a single pillar was presented before and after the experimental conditions. We rotated all trajectories such that the x axis points from the origin to the center of mass of the targets. To visualize trajectories in the various experimental conditions, we created time-normalized (proportion of maximum across a sliding time window) density maps. We then folded the data about the line of symmetry, $y = 0$, and applied a density threshold to the time-normalized density map. A piecewise phase transition function was then fit to quantify the bifurcation:

$$y = \begin{cases} 0 & x \leq x_c \\ A|x - x_c|^{\alpha} & x > x_c \end{cases},$$ [4]

where x_c is the critical point, α is the critical exponent, and A is the proportionality constant. We also performed randomization tests for each bifurcation where we conducted the exact fit procedure described above to data where the trajectories were randomized by keeping the x coordinates and swapping the y coordinates with values from other random events. Randomizations show that the resultant fit to our experimental data was highly significant ($P < 0.01$ for binary choice and $P < 10^{-4}$ for the three-choice case).

Based on the amount of time it took flies to reach one of the available targets, we also classified individual fly tracks into one of two categories—direct tracks and nondirect tracks (60) (*SI Appendix*, Fig. S11 *A* and *H* has details). In our model, the direct tracks were also accounted for by varying the directional tuning of spins. A high neural tuning (low ν) results in more directed tracks (*SI Appendix*, Fig. S14).

Locust Virtual Reality Experiments. All experiments were conducted on 156 instar 5 desert locusts (*S. gregaria*; 57 individuals for two-choice experiments and 99 individuals for three-choice experiments, respectively) raised in the Animal Research Facility of the University of Konstanz. Based on our filtering criteria, 122 of 156 locusts were used in our analyses. Experiments were conducted in a locust virtual reality setup procured from loopbio GmbH (28). The experimental procedure was identical to the one described above for flies, except now, each experimental trial lasted 48 min—three experimental sets (12 min each) and two control sets (6 min each). Analyzing bifurcations in locust trajectories using the same methods described above showed that the resultant bifurcations fit to our experimental data were highly significant ($P < 0.01$ for binary choice and $P < 10^{-4}$ for the three-choice case).

Similar to the flies, the locust trajectories were also classified as direct or nondirect tracks. However, because the locust virtual reality system allowed the animals to stop and reconsider movement during the decision-making process, we added an additional category to the classification of individual locust tracks viz. the wandering tracks (*SI Appendix*, Fig. S12 *A* and *J* has details).

Fish Virtual Reality Experiments. All experiments were conducted on 1- $\pm$ 0.1-cm-long zebrafish (*D. rerio*) of age 24 to 26 d postfertilization raised in a room at 28 °C on a 16-h light, 8-h dark cycle; 440 fish were tested in total. Of these, 198 fish were exposed to decision-making with two virtual targets, 39 fish were exposed to decision-making with three equidistant virtual targets, and 50 fish were exposed to decision-making with three targets in asymmetric geometry (*SI Appendix* has more details). Experiments were conducted in a fish virtual reality setup procured from loopbio GmbH (refer to ref. 28 for details). After a fish was introduced in the arena, it was given 20 min to acclimatize to the environment. This was followed by a 10-min control, where it was presented with a single virtual conspecific circling the arena in a circle of radius 8 cm. After this, for experiments in symmetric geometries, the real fish was exposed to choice experiments that lasted 90 min with the virtual fish initialized with random lateral distances between them and random swim direction. To visualize the bifurcations, we normalized (proportion of maximum) and stacked the marginal distributions along the direction of the virtual fish's motion for various lateral distances. For experiments in asymmetric geometries, the real fish was exposed to choice experiments where distance between the center virtual fish and its closer neighbor was 0.03 m and its distance to the other neighbor was 0.09 m (Fig. 4). All experiments were conducted in accordance with the animal ethics permit approved by Regierungspräsidium Freiburg, G-17/170.

Data Availability. Animal movement data have been deposited in GitHub (https://github.com/vivekhsridhar/GODM) and Zenodo (DOI: 10.5281/zenodo. 5599711) (61)

ECOLOGY

BIOPHYSICS AND
COMPUTATIONAL BIOLOGY

Sridhar et al.
The geometry of decision-making in individuals and collectives

PNAS | 7 of 8
https://doi.org/10.1073/pnas.2102157118

1. C. E. J. Kennedy, J. A. Endler, S. L. Poynton, H. McMinn, Parasite load predicts mate choice in guppies. *Behav. Ecol. Sociobiol.* **21**, 291–295 (1987).
2. K. Summers, R. Symula, M. Clough, T. Cronin, Visual mate choice in poison frogs. *Proc. Biol. Sci.* **266**, 2141–2145 (1999).
3. E. Forsgren, Predation risk affects mate choice in a Gobiid fish. *Am. Nat.* **140**, 1041–1049 (1992).
4. R. Kiani, L. Corthell, M. N. Shadlen, Choice certainty is informed by both evidence and decision time. *Neuron* **84**, 1329–1342 (2014).
5. J. M. Beck *et al.*, Probabilistic population codes for Bayesian decision-making. *Neuron* **60**, 1142–1152 (2008).
6. A. K. Churchland, R. Kiani, M. N. Shadlen, Decision-making with multiple alternatives. *Nat. Neurosci.* **11**, 693–702 (2008).
7. S. S. Kim, H. Rouault, S. Druckmann, V. Jayaraman, Ring attractor dynamics in the *Drosophila* central brain. *Science* **356**, 849–853 (2017).
8. J. D. Seelig, V. Jayaraman, Neural dynamics for landmark orientation and angular path integration. *Nature* **521**, 186–191 (2015).
9. J. S. Taube, R. U. Muller, J. B. Ranck Jr., Head-direction cells recorded from the postsubiculum in freely moving rats. II. Effects of environmental manipulations. *J. Neurosci.* **10**, 436–447 (1990).
10. A. Finkelstein *et al.*, Three-dimensional head-direction coding in the bat brain. *Nature* **517**, 159–164 (2015).
11. A. Sarel, A. Finkelstein, L. Las, N. Ulanovsky, Vectorial representation of spatial goals in the hippocampus of bats. *Science* **355**, 176–180 (2017).
12. Ø. A. Høydal, E. R. Skytøen, S. O. Andersson, M. B. Moser, E. I. Moser, Object-vector coding in the medial entorhinal cortex. *Nature* **568**, 400–404 (2019).
13. R. Wehner, B. Michel, P. Antonsen, Visual navigation in insects: Coupling of egocentric and geocentric information. *J. Exp. Biol.* **199**, 129–140 (1996).
14. A. Bahl, F. Engert, Neural circuits for evidence accumulation and decision-making in larval zebrafish. *Nat. Neurosci.* **23**, 94–102 (2020).
15. I. Pinkoviezky, I. D. Couzin, N. S. Gov, Collective conflict resolution in groups on the move. *Phys. Rev. E* **97**, 032304 (2018).
16. K. Zhang, Representation of spatial orientation by the intrinsic dynamics of the head-direction cell ensemble: A theory. *J. Neurosci.* **16**, 2112–2126 (1996).
17. D. S. Touretzky, "Attractor network models of head direction cells" in *Head Direction Cells and the Neural Mechanisms of Spatial Orientation*, S. I. Wiener, J. S. Taube, Eds. (MIT Press, Cambridge, MA, 2005), pp. 411–432.
18. X. Sun, M. Mangan, S. Yue, "An analysis of a ring attractor model for cue integration" in *Conference on Biomimetic and Biohybrid Systems* (Springer, 2018), pp. 459–470.
19. L. C. York, M. C. W. van Rossum, Recurrent networks with short term synaptic depression. *J. Comput. Neurosci.* **27**, 607–620 (2009).
20. B. Collignon, A. Séguret, J. Halloy, A stochastic vision-based model inspired by zebrafish collective behaviour in heterogeneous environments. *R. Soc. Open Sci.* **3**, 150473 (2016).
21. L. Benedetti-Cecchi, L. Tamburello, E. Maggi, F. Bulleri, Experimental perturbations modify the performance of early warning indicators of regime shift. *Curr. Biol.* **25**, 1867–1872 (2015).
22. A. Gelblum *et al.*, Ant groups optimally amplify the effect of transiently informed individuals. *Nat. Commun.* **6**, 7729 (2015).
23. B. M. McCoy, T. T. Wu, *The Two-Dimensional Ising Model* (Courier Corporation, ed. 2, 2014).
24. J. M. Choi, A. S. Holehouse, R. V. Pappu, Physical principles underlying the complex biology of intracellular phase transitions. *Annu. Rev. Biophys.* **49**, 107–133 (2020).
25. A. A. Hyman, K. Simons, Cell biology. Beyond oil and water—phase transitions in cells. *Science* **337**, 1047–1049 (2012).
26. A. Strandburg-Peshkin, D. R. Farine, I. D. Couzin, M. C. Crofoot, GROUP DECISIONS. Shared decision-making drives collective movement in wild baboons. *Science* **348**, 1358–1361 (2015).
27. R. Ratcliff, P. L. Smith, S. D. Brown, G. McKoon, Diffusion decision model: Current issues and history. *Trends Cogn. Sci.* **20**, 260–281 (2016).
28. J. R. Stowers *et al.*, Virtual reality for freely moving animals. *Nat. Methods* **14**, 995–1002 (2017).
29. T. Poggio, W. Reichardt, A theory of the pattern induced flight orientation of the fly *Musca domestica*. *Kybernetik* **12**, 185–203 (1973).
30. D. Varju, Stationary and dynamic responses during visual edge fixation by walking insects. *Nature* **255**, 330–332 (1975).
31. W. Reichardt, T. Poggio, A theory of the pattern induced flight orientation of the fly *Musca domestica* II. *Biol. Cybern.* **18**, 69–80 (1975).
32. P. K. Kaushik, M. Renz, S. B. Olsson, Characterizing long-range search behavior in Diptera using complex 3D virtual environments. *Proc. Natl. Acad. Sci. U.S.A.* **117**, 12201–12207 (2020).
33. E. Horn, R. Wehner, The mechanism of visual pattern fixation in the walking fly, *Drosophila melanogaster*. *J. Comp. Physiol. A Neuroethol. Sens. Neural Behav. Physiol.* **101**, 39–56 (1975).
34. G. K. Wallace, Some experiments on form perception in the nymphs of the desert locust, *Schistocerca gregaria forskaal*. *J. Exp. Biol.* **35**, 765–775 (1958).
35. P. T. Gonzalez-Bellido, T. J. Wardill, M. Juusola, Compound eyes and retinal information processing in miniature dipteran species match their specific ecological demands. *Proc. Natl. Acad. Sci. U.S.A.* **108**, 4224–4229 (2011).
36. O. Faivre, M. Juusola, Visual coding in locust photoreceptors. *PLoS One* **3**, e2173 (2008).
37. M. Wilson, Angular sensitivity of light and dark adapted locust retinula cells. *J. Comp. Physiol.* **97**, 323–328 (1975).
38. G. A. Linneweber *et al.*, A neurodevelopmental origin of behavioral individuality in the *Drosophila* visual system. *Science* **367**, 1112–1119 (2020).
39. F. R. Kiral *et al.*, Variable brain wiring through scalable and relative synapse formation in *Drosophila*. bioRxiv [Preprint] (2021). https://www.biorxiv.org/content/10.1101/2021.05.12.443860v1 (Accessed 20 July 2021).
40. S. M. Buchanan, J. S. Kain, B. L. de Bivort, Neuronal control of locomotor handedness in *Drosophila*. *Proc. Natl. Acad. Sci. U.S.A.* **112**, 6700–6705 (2015).
41. I. D. Couzin, J. Krause, N. R. Franks, S. A. Levin, Effective leadership and decision-making in animal groups on the move. *Nature* **433**, 513–516 (2005).
42. B. Nabet, N. E. Leonard, I. D. Couzin, S. A. Levin, Dynamics of decision-making in animal group motion. *J. Nonlinear Sci.* **19**, 399–435 (2009).
43. N. E. Leonard *et al.*, Decision versus compromise for animal groups in motion. *Proc. Natl. Acad. Sci. U.S.A.* **109**, 227–232 (2012).
44. R. Gray, A. Franci, V. Srivastava, N. E. Leonard, Multiagent decision-making dynamics inspired by honeybees. *IEEE Trans. Control Netw. Syst.* **5**, 793–806 (2018).
45. A. Bizyaeva, A. Franci, N. E. Leonard, A general model of opinion dynamics with tunable sensitivity. arXiv [Preprint] (2020). https://arxiv.org/abs/2009.04332v1 (Accessed 20 July 2021).
46. I. D. Couzin *et al.*, Uninformed individuals promote democratic consensus in animal groups. *Science* **334**, 1578–1580 (2011).
47. D. Biro, D. J. T. Sumpter, J. Meade, T. Guilford, From compromise to leadership in pigeon homing. *Curr. Biol.* **16**, 2123–2128 (2006).
48. I. D. Couzin, J. Krause, R. James, G. D. Ruxton, N. R. Franks, Collective memory and spatial sorting in animal groups. *J. Theor. Biol.* **218**, 1–11 (2002).
49. C. W. Reynolds, "Flocks, herds and schools: A distributed behavioral model" in *Proceedings of the 14th Annual Conference on Computer Graphics and Interactive Techniques* (Association for Computing Machinery, New York, NY, 1987), pp. 25–34.
50. T. Vicsek, A. Czirók, E. Ben-Jacob, I. Cohen, O. Shochet, Novel type of phase transition in a system of self-driven particles. *Phys. Rev. Lett.* **75**, 1226–1229 (1995).
51. C. C. Ioannou, M. Singh, I. D. Couzin, Potential leaders trade off goal-oriented and socially oriented behavior in mobile animal groups. *Am. Nat.* **186**, 284–293 (2015).
52. A. Perna *et al.*, Individual rules for trail pattern formation in Argentine ants (*Linepithema humile*). *PLoS Comput. Biol.* **8**, e1002592 (2012).
53. S. Amari, Homogeneous nets of neuron-like elements. *Biol. Cybern.* **17**, 211–220 (1975).
54. S. Amari, Dynamics of pattern formation in lateral-inhibition type neural fields. *Biol. Cybern.* **27**, 77–87 (1977).
55. K. S. Kakaria, B. L. de Bivort, Ring attractor dynamics emerge from a spiking model of the entire protocerebral bridge. *Front. Behav. Neurosci.* **11**, 8 (2017).
56. L. Peliti, *Statistical Mechanics in a Nutshell* (Princeton University Press, 2011).
57. J. J. Hopfield, Neural networks and physical systems with emergent collective computational abilities. *Proc. Natl. Acad. Sci. U.S.A.* **79**, 2554–2558 (1982).
58. K. G. Wilson, The renormalization group and critical phenomena. *Rev. Mod. Phys.* **55**, 583 (1983).
59. E. Schneidman, M. J. Berry II, R. Segev, W. Bialek, Weak pairwise correlations imply strongly correlated network states in a neural population. *Nature* **440**, 1007–1012 (2006).
60. S. Takagi, R. Benton, Animal behavior: A neural basis of individuality. *Curr. Biol.* **30**, R710–R712 (2020).
61. V. H. Sridhar *et al.*, vivekhsridhar/GODM: GODM v0.1. Zenodo. https://zenodo.org/record/5599712#.YZ44SfHMJmA. Deposited 26 October 2021.

8 of 8 | **PNAS**
https://doi.org/10.1073/pnas.2102157118

Sridhar et al.
The geometry of decision-making in individuals and collectives